

CH₄-to-CH₃OH on Mononuclear Cu(II) Sites Supported on Al₂O₃: Structure of Active Sites from Electron Paramagnetic Resonance

Jordan Meyet, Anton Ashuiev, Gina Noh, Mark A. Newton, Daniel Klose, Keith Searles, Alexander P. van Bavel, Andrew D. Horton, Gunnar Jeschke, Jeroen A. van Bokhoven*, Christophe Copéret*

J. Meyet, A. Ashuiev, Dr. G. Noh, Dr. M. A. Newton, Dr. D. Klose, Dr. K. Searles, Prof. Dr. G. Jeschke, Prof. Dr. C. Copéret, Prof. Dr. J. A. van Bokhoven

Department of Chemistry and Applied Biosciences, ETH Zurich

Vladimir-Prelog-Weg 1-5, 8093 Zürich, Switzerland

E-mail: ccoperet@ethz.ch

Prof. Dr. J. A. van Bokhoven

Laboratory for Catalysis and Sustainable Chemistry, Paul Scherrer Institute Villigen 5232, Switzerland

E-mail: jeroen.vanbokhoven@chem.ethz.ch

Dr. A. P. van Bavel, Dr. A. D. Horton

Shell Global Solutions International B.V.

Grasweg 31, 1031 HW Amsterdam, The Netherlands

ABSTRACT: The selective conversion of methane to methanol remains one of the holy grails of chemistry, where Cu-exchanged zeolites have been shown to selectively convert methane to methanol under stepwise conditions. Over the years, several active sites have been proposed, ranging from mono-, di- to trimeric Cu(II). Herein, we report the formation of well-dispersed monomeric Cu(II) species supported on alumina using surface organometallic chemistry and their reactivity towards the selective and stepwise conversion of methane to methanol. Extensive studies using various transition alumina supports combined with spectroscopic characterization, in particular electron paramagnetic resonance (EPR), show that the active sites are associated with specific facets, which are typically found in γ - and η -alumina phase, and that their EPR signature can be attributed to species having a tri-coordinated $[(\text{Al}_2\text{O})\text{Cu}^{\text{II}}\text{O}(\text{OH})]^-$, T-shape geometry. Overall, the selective conversion of methane to methanol, a two-electron process, involves two monomeric Cu(II) sites that play in concert.

Introduction

The direct and selective conversion of CH₄ to CH₃OH could transform the petrochemical industry, by enabling on-site conversion of CH₄ on a scale much smaller than is currently viable. Existing routes, which are both energy-

intensive and indirect, require the generation of syngas (H_2/CO) through CH_4 reforming, which can then be converted to CH_3OH . Cheap and abundant CH_4 is the main constituent of natural gas (70-90 %), but its transportation in liquid form is energy demanding and comes at additional cost. Although the development of catalytic processes for the partial oxidation of CH_4 is highly desirable, this reaction remains challenging due to the low reactivity of CH_4 compared to that of CH_3OH which leads to facile generation of over-oxidized and unwanted products (e.g. CO , CO_2).¹⁻⁴ In nature, methane monooxygenases (MMOs, with either Fe or Cu active sites) are highly efficient at performing this selective oxidation.⁵ The particulate form of this enzyme (pMMO) possesses several copper-containing sites for which the exact structure and nuclearity are still under debate.⁶⁻⁸ Initial studies ascribed the active site as a dimeric copper species present in the Pmmob subunit (Cu_B , Fig. 1a)⁹. A more recent report, supported by electron paramagnetic resonance (EPR) spectroscopy, however, has shown the exclusive presence of mononuclear sites in pMMO; the Cu_C site located in the Pmmoc subunit has been assigned to the metal binding site responsible for hydrocarbon binding and oxidation (Fig. 1a).⁸

In parallel, promising processes based on inorganic materials have been developed in recent years. These processes rely on chemical looping, which decouples an aerobic (O_2) oxidation step from the CH_4 activation step, and therefore curtails over-oxidation of the methoxy species formed.^{10,11} The most-studied materials within the chemical looping paradigm are copper-exchanged zeolites. Different types of active centers have been proposed based on spectroscopic characterization.¹² These proposals include a dinuclear mono- μ -oxo $[\text{Cu}-\text{O}-\text{Cu}]^{2+}$ center¹³ (Fig. 1a) and a trinuclear $[\text{Cu}_3\text{O}_3]^{2+}$ core.¹⁴ In addition, monomeric Cu sites $[\text{CuOH}]^+$ in chabazite,¹⁵ and two monomers present in mordenite have been proposed based on density functional theory (DFT) calculations¹⁶. Recently, the formation of paired monomeric $[\text{CuOH}]^+$ in zeolite Omega has been reported using anomalous X-ray diffraction.¹⁷ However, despite major efforts, the active site structures remain highly debated. This deficit notwithstanding, substantial improvements in CH_3OH yield per chemical looping cycle have been achieved to reach the theoretical limit of CH_3OH for two Cu(II) sites.¹⁸ However, state-of-the-art zeolite-based materials remain economically unviable for commercial applications because of an insufficient amount of reactive sites per unit mass and the long cycle times associated with this step-wise process.^{19,20} Thus, alternate materials must be explored for this challenging transformation. While the discovery of more efficient materials is of great importance to overcome some limitations faced by zeolites materials, the identification and characterization of the reactive centers is required to provide a structure/reactivity relationship as a guideline to improve material performance. Among possible alternative materials explored, copper supported on silica is shown to produce CH_3OH ,²¹⁻²³ however the obtained yield is low and the active sites are ill-defined (small CuO clusters).

Recently, we showed that proximal monomeric Cu(II) sites on alumina in an aluminosilicate environment, that resembled this of zeolites, could convert CH_4 to CH_3OH .²⁴ The material was generated via the surface organometallic chemistry (SOMC) and thermolytic molecular precursor (TMP) approach,²⁵ allowing the formation of highly-dispersed Cu(II) centers with a coordination sphere dictated by the choice of tailored molecular precursor. However, the mixed (Si/Al) surface environment arising from the use of Cu(II) siloxide precursors, necessary to reproduce the chemical environment found in zeolites, also led to the formation of multiple sites and prevented to obtain any detailed structural characterization of the reactive Cu(II) sites.

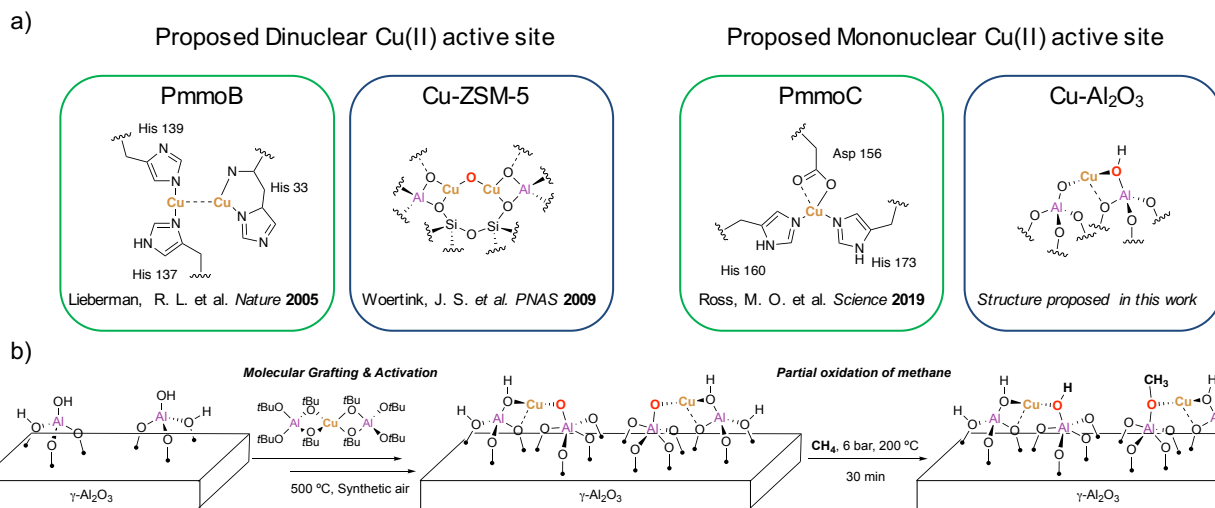


Figure 1. a) Proposed dinuclear (left) and mononuclear (right) active sites in the enzyme Pmmo (green frame) and the equivalent (in terms of copper nuclearity) analogs proposed for Cu supported on oxide supports (blue frame); **b)** Schematic illustration of the strategy used to generate monomeric Cu(II) sites in a pure alumina environment and the subsequent reaction with CH₄ to form hydroxy and methoxy species.

We thus reasoned that the formation of well-dispersed Cu(II) in a pure alumina environment, using a copper-aluminate molecular precursor, would enable the identification of the active site structure while keeping the high reactivity of these Cu(II) sites (Fig. 1b) even if the reactivity of Cu(II) centers in a pure aluminum environment is yet to be explored.

Here we describe the formation of well-dispersed Cu(II) sites on transitional alumina using the SOMC/TMP approach, disclose their reactivity towards the selective conversion of methane to methanol, and identify the structure of the active sites. In particular, *in situ* EPR spectroscopy allows for the spectroscopic identification of reactive Cu(II) surface sites involved in the selective partial oxidation of CH₄. These reactive sites display a unique EPR signature, which can be observed for Cu(II) on γ -, η - and θ -Al₂O₃ but not for non-defective α -Al₂O₃. Combining X-ray absorption spectroscopy (XAS), advanced EPR methods and computational modeling enabled the assignment of the reactive monomeric Cu(II) sites on alumina as a tri-coordinated [(Al₂O)CuO(OH)]⁺ species.

Results

Formation of Cu monomers on γ -alumina

The copper aluminate molecular precursor,²⁶ [Cu(κ^2 -Al(O*t*Bu)₄)₂] (**1**) (see ESI Section 3, Figs. S1 - S5 for the full characterization of **1**) was grafted on γ -Al₂O₃ (“ γ -a”) dehydroxylated under vacuum at varied temperatures (denoted by X in degree Celsius in “ γ -a_X”): γ -a₅₀₀ (OH density, Θ = 2.4 OH.nm⁻²), γ -a₇₀₀ (Θ = 0.9 OH.nm⁻²) and γ -a₈₀₀ (Θ = 0.4 OH.nm⁻²) (see also ESI Figs. S6 & S7), to yield the corresponding grafted materials **1- γ -a_X**. These grafted materials were characterized by UV-vis, diffuse reflectance infrared (DRIFTS), EPR and X-ray absorption near-edge spectroscopies (XANES) (ESI Section 4 & Figs. S7 – S9). All **1- γ -a_{X00}** materials show similar spectroscopic features, indicating the generation of similar surface species after grafting irrespective of the initial dehydroxylation temperature for γ -Al₂O₃. The presence of Cu(II) was confirmed by both EPR and the observation in the electronic spectra of the d-d transition characteristic of Cu(II) species. However, the presence of a pre-edge feature at 8983

eV in the XANES, characteristic of Cu(I) species, indicates the partial reduction of Cu (Fig. S9), as previously observed when different Cu(II) precursors were grafted on alumina.²⁴

Thermal activation of these **1- γ -a_x** materials under a flow of dry synthetic air at 500 °C leads to the exclusive generation of organic-free Cu(II) surface species (**1₅₀₀- γ -a_x**), as demonstrated by IR, UV-Vis, EPR and XANES (Section 4, Figs. S10 – S12). Possible auto-reduction of the Cu center under thermal activation, as previously reported for zeolitic materials,^{27,28} can be excluded as no pre-edge features for Cu(I) could be observed in the XANES spectra (Fig. S12). Continuous wave (CW) X-band EPR analysis of the activated material (Fig. S12) shows the presence of paramagnetic Cu(II) species in a nearly axial environment ($g_{\parallel} > g_{\perp} > g_e$) with well-resolved Cu hyperfine coupling, which confirms the presence of monomeric Cu(II) species well-dispersed on the alumina support.²⁴ Comparison of the CW EPR spectra amongst the activated Cu generated on the partially dehydroxylated alumina at different temperatures (*vide infra*), allows the identification of at least two different Cu species based on the observed parallel transitions (A_{\parallel} and g_{\parallel}): $A_{\parallel} \approx 370$ MHz and $g_{\parallel} \approx 2.39$ for one site (denoted site I) and $A_{\parallel} \approx 440$ MHz and $g_{\parallel} \approx 2.33$ for the remainder of the signal (denoted site II, but which is composed of multiple species; *vide infra*) (Fig. S12). The ratio between these two sites is highly dependent on the initial dehydroxylation temperature of the alumina support prior to grafting. A dehydroxylation temperature of 500°C (**1₅₀₀- γ -a₅₀₀**) yields predominantly site I, whereas dehydroxylation at 800°C (**1₅₀₀- γ -a₈₀₀**) gives primarily site II.

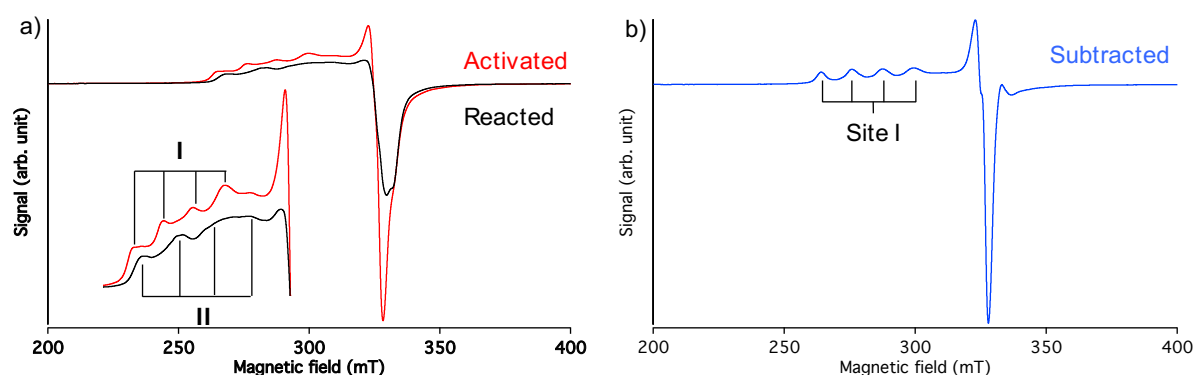


Figure 2. a) *In situ* X-band EPR spectra (298 K) for **1₅₀₀- γ -a₅₀₀** before and after reaction under 6 bar of CH₄ for 30 min at 200 °C **b)** X-band EPR difference spectrum (298 K) before-after reaction

Reactivity of the material

The activated materials, **1₅₀₀- γ -a_x**, were reacted under 6 bars of CH₄ at 200°C for 30 min and isolated under inert conditions for further spectroscopic characterization. DRIFTS analysis after reaction shows the appearance of two bands at 2957 and 2853 cm⁻¹ assigned to the asymmetric and symmetric stretch of methoxy surface species, respectively (Fig. S13).²⁹ This assignment was confirmed by ¹³C solid-state nuclear magnetic resonance (SSNMR) of **1₅₀₀- γ -a₅₀₀** reacted with ¹³CH₄, where two distinct peaks are observed in the ¹³C NMR spectra: a major broad peak at 48.3 ppm along with a minor peak at 64 ppm, assigned respectively to surface methoxy/methanol (CH₃O(H)-) and small amounts of dimethyl ether (DME) (Fig. S14).³⁰

122 After extraction with water at 120 °C, the **1₅₀₀-γ-a₅₀₀** material shows the highest CH₃OH productivity among all
 123 samples with 0.12 mol CH₃OH/mol of Cu. The CH₃OH yields for the other materials are lower, with **1₅₀₀-γ-a₈₀₀**
 124 yielding only half the amount of CH₃OH (0.06 mol CH₃OH/mol of Cu; ESI Table 1). A recycling study was also
 125 performed using **1-γ-a₇₀₀** calcined at 700 °C (**1₇₀₀-γ-a₇₀₀**) showing similar CH₃OH yields before and after recycling
 126 with ca. 0.09 CH₃OH/mol of Cu (ESI Table S1). The reaction of γ-Al₂O₃ in the absence of Cu sites under similar
 127 conditions does not yield any CH₃OH products.²⁴

128 To understand the origin of the observed reactivity, the reaction with CH₄ was monitored by *in situ* EPR spectroscopy (Fig. 2a). For all materials, the initial spectra include a mixture of sites, while after reaction only the signal
 129 associated with site I completely disappears, leaving a broad signal consisting of a distribution of unreactive Cu
 130 monomers described as site II (Figs. 2a, S15–S16). The partial disappearance of the EPR signal can be rationalized
 131 by the reduction of reactive Cu(II) species to EPR-silent Cu(I). Furthermore spin quantification, obtained from
 132 double integrals of the signal before and after reaction, is consistent with the expected number of electrons (2 e⁻ for
 133 CH₄ to CH₃OH) required for the selective reaction with CH₄ (Fig. 3a).²⁴ This Cu(II)/Cu(I) redox process is further
 134 evidenced by Cu K-edge XANES analysis of material **1₅₀₀-γ-a₅₀₀** before and after reaction, which shows the emer-
 135 gence of a Cu(I) pre-edge feature (Fig. S17) similar to previous reports for zeolitic-³¹ and alumina-based systems.²⁴
 136 Thus, the EPR signal of the reactive Cu(II) species can be obtained by subtracting the spectra between the reacted
 137 and unreacted materials, revealing the spectroscopic signature of the reactive monomeric Cu(II) site (site I). In
 138 contrast to many spectroscopic techniques, which characterize both reactive and spectator Cu(II) sites, this EPR
 139 signature belongs exclusively to the reactive centers involved in the redox reaction.

140 The maximum ratio of reduced Cu(II), determined from the double integrals of the signals before and after reaction,
 141 was observed for **1₅₀₀-γ-a₅₀₀** with 32 % of Cu(I) formed for a CH₃OH yield of 0.12 mol CH₃OH/mol of Cu (Fig. 3a).
 142 Additional information regarding the amount of Cu(II) centers reduced upon reaction with CH₄ was obtained from
 143 linear combination analysis (LCA) of the XANES spectra for **1₅₀₀-γ-a₅₀₀**; it corresponds to ca. 44 % of Cu(I) formed
 144 upon reaction with methane. The higher proportion of reduced Cu centers obtained from LCA analysis compared
 145 to the one obtained by EPR spectroscopy suggests the presence of a small amount of EPR silent reactive Cu(II)
 146 centers, possibly associated with the presence of small antiferromagnetically coupled Cu(II)-oxo clusters.³²

147 To further investigate the presence of small multimetric Cu(II)-oxo centers, the material was characterized by
 148 EXAFS spectroscopy. Cu K-edge EXAFS analysis of **1₅₀₀-γ-a₅₀₀** by (Fig. S18, Table S2) indicates an average of 3
 149 O in the first coordination sphere of the Cu center and, crucially, the absence of a Cu-Cu path consistent with the
 150 presence of mostly Cu(II) monomers. Comparing the first shell between the initial and reacted states does not reveal
 151 significant changes in the local Cu–O coordination sphere (Fig. S18, Table S2). Despite the absence of Cu-O-Cu
 152 scattering in the deconvolution of the EXAFS, the presence of minor contributions of multimetric Cu(II) species
 153 cannot be excluded.

154 Further interpretation of the EXAFS is, however, limited by a relatively reduced dataset and low signal-to-noise
 155 ratio. Moreover, EXAFS averages over all (both active and inactive) Cu species present; and, in these cases these
 156 different contributions cannot be disentangled with any degree of precision or specificity.

By contrast, EPR spectroscopy permits more selective probing of the reactive site (*vide supra*). Taking advantage of the specificity of this spectroscopy, a wider range of transitional alumina supports was explored (η -, θ - and α - Al_2O_3) to better understand the formation and identity of this reactive monomeric Cu species. Transition aluminas provide different anchoring sites on the support by exposing different low-index planes and facets, although the nature of specific facets remains a matter of debate. The γ - and η - Al_2O_3 phases are of particular interest because of their high Lewis acidity and similar reactivity.³³ In fact, both are able to coordinate N_2 with a blue shifted IR band at 2355 cm^{-1} , assigned to adsorption at tri-coordinated Al (Al_{III}) for γ - Al_2O_3 .³⁴ Such highly Lewis acidic undercoordinated sites are absent on α - Al_2O_3 surface.

Similar grafting and activation procedures were applied for these different transition aluminas, leading to the generation of well-dispersed Cu(II) species (Figs. S19 – S24) supported on Al_2O_3 , $\mathbf{1}_{500}\text{-z-a}_x$ (where “z” denotes the phase of the transition alumina employed). Post reaction with CH_4 , the surface speciation for each of these materials, was again probed using DRIFTS (Fig. S25). Material reactivity was assessed by *in situ* EPR spectroscopy, coupled with CH_3OH quantification (Figs. S26 – S30, Table S3). In all cases, except for $\mathbf{1}_{500}\text{-}\alpha\text{-a}_{500}$, only sites I and II were observed in EPR spectra of the activated material (Figs. S26-S29). Upon reaction with CH_4 , only site I disappeared. For $\mathbf{1}_{500}\text{-}\alpha\text{-a}_{500}$, CH_3OH could not be quantified, and the low intensity EPR signal observed for Cu(II) (Fig. S30), likely due to the very low specific surface area ($3\text{ m}^2\cdot\text{g}^{-1}$) and the small amounts of supported Cu, is unperturbed by reaction with CH_4 . The CH_3OH yield measured for all other materials, however, correlates with the disappearance of EPR signal (Fig. 3a) as was previously observed in the case of $\mathbf{1}_{500}\text{-}\gamma\text{-a}_x$.

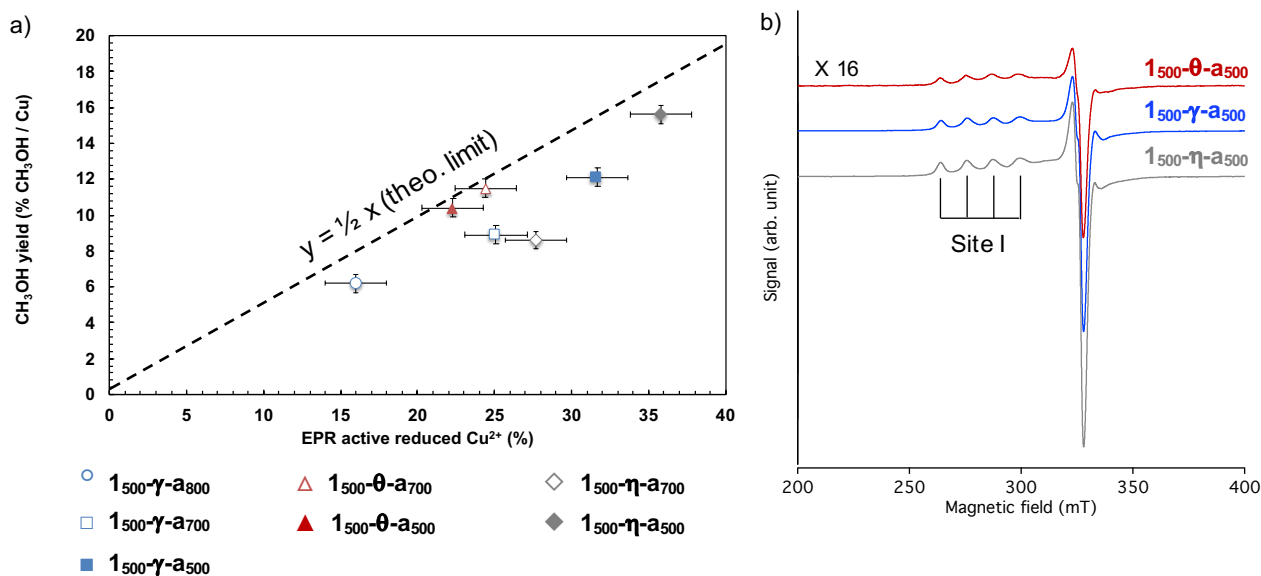
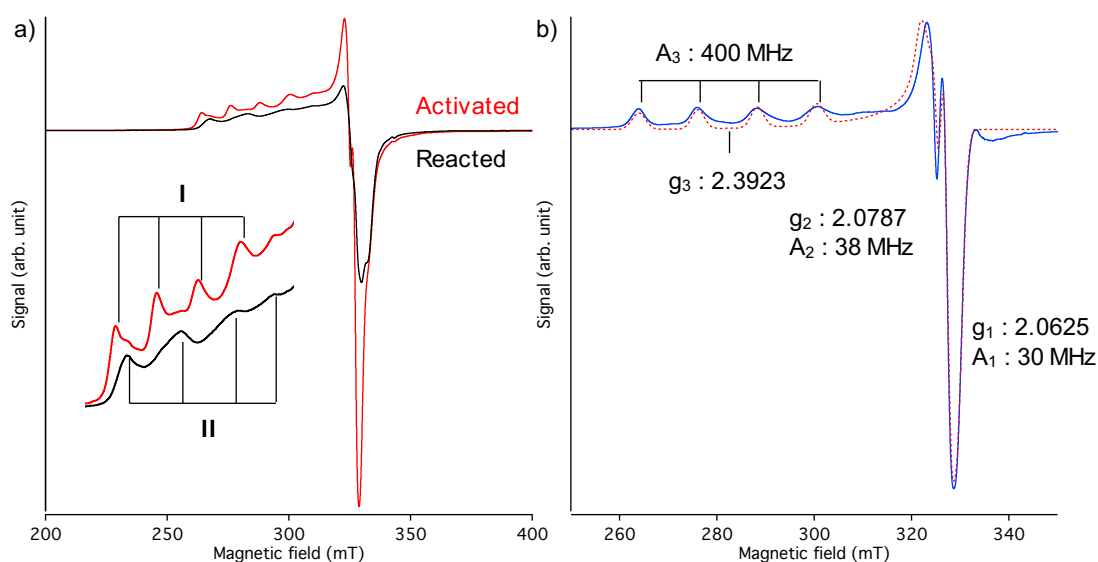


Figure 3. a) Reducibility of the monomeric Cu site determined by double integration of EPR *in situ* reaction (in % of Cu) versus CH_3OH yield obtained after reaction with CH_4 in mol $\text{CH}_3\text{OH}/\text{mol}$ of Cu, for the different Cu supported transitional aluminas tested. Deviation from the theoretical limit (dash line), indicating the 2 electrons required for the formation of CH_3OH , provides information on the material selectivity toward CH_3OH , and **b)** X-band difference EPR spectra (298 K) before-after reaction of $\mathbf{1}_{500}\text{-a}_{500}$ supported on various transitional alumina displaying identical reactive Cu(II) monomeric site I.

183 Greater reactivity is observed for **1₅₀₀- η -a₅₀₀** (0.16 mol CH₃OH/mol Cu), compared to that for **1₅₀₀- γ -a₅₀₀** (0.12 mol
 184 CH₃OH/mol Cu), which could be rationalize by higher Lewis acidity for **η -a₅₀₀** compared to **γ -a₅₀₀**, and the presence
 185 of greater amounts of defective undercoordinated aluminum (Al_{III}) surface sites. These Al_{III}, and their relative
 186 amounts, are evidenced by the area of the band of coordinated N₂ observed in the IR spectra of the dehydroxylated
 187 Al₂O₃ (Fig. S19). This enhanced reactivity suggests that Cu sites are located in close proximity to surface Al_{III}
 188 defective sites.^{35–37}

189 Low-temperature CW EPR, and simulation of the EPR parameters, was performed for **1₅₀₀- η -a₅₀₀**, which possesses
 190 the highest fraction of reactive site I. The EPR spectra of the activated and reacted material for **1₅₀₀- η -a₅₀₀** (Fig. 4a)
 191 are similar to those observed for **1₅₀₀- γ -a₅₀₀**. The resulting difference spectra, corresponding to the reactive, nearly
 192 axial, monomeric Cu(II) species observed on all the materials studied, can be simulated with the g tensor parameters
 193 g (site I) = [2.0625 2.0787 2.3923], and hyperfine coupling A_{Cu} (MHz) = [30 38 400] (Fig. 4b), while the inactive
 194 sites (site II) correspond to a mixture of at least two distinct species (ESI Fig. S31).



195
 196 **Figure 4. a)** X-Band EPR spectrum (103 K) for **1₅₀₀- η -a₅₀₀** before and after reaction under 6 bar of CH₄ for 30 min at 200 °C,
 197 and **b)** X-Band EPR difference spectrum (103 K) for **1₅₀₀- η -a₅₀₀** before-after reaction (plain) and the resulting simulation
 198 (dashed) parametrizing the spectrum of the active species.

199
 200 To further characterize the reactive species, **1₅₀₀- γ -a₅₀₀** was contacted with CO as a probe molecule and monitored
 201 by IR and EPR (Figs. S32 & S33). After introduction of 110 mbar of CO, followed by evacuation, new features are
 202 observed by IR in the range of 1700 – 1200 cm⁻¹. The difference between the reacted and activated spectra reveal
 203 the appearance of bands at 3611 cm⁻¹ (ν_{OH}), 1647 cm⁻¹ (ν_{sOCO}), 1479 cm⁻¹ (ν_{sOCO}), 1443 cm⁻¹ (ν_{sOCO}), 1233 cm⁻¹ (δ_{OH})
 204 (Fig. 5a & Fig. S32). These bands are associated with stable bicarbonate (HOCO₂⁻) surface intermediates formed
 205 during the oxidation of CO, as previously reported for the interaction of CO₂ with γ -Al₂O₃.³⁸ The same experiment
 206 monitored by EPR spectroscopy results in partial disappearance of site I along with appearance of a new EPR signal
 207 (Fig. 5b & Fig. S33). Difference spectra confirm the involvement of the reactive monomeric Cu(II) site for the one-
 208 electron oxidation of CO to a HOCO₂[•] radical anion. Similar reactivity was observed for **1₅₀₀- η -Al₂O_{3.500}** under

identical conditions (Fig. S34). The new signal, which has an effective g value of 2.0026, possesses an effective super-hyperfine coupling of 50 MHz, as determined from simulation (Fig. 5c). The presence of 11 lines for the radical species formed can be explained by hyperfine interaction between the radical center with two equivalent Al nuclei ($A_{\text{eff}}(^{27}\text{Al}) = 50 \text{ MHz}$). Similar super-hyperfine couplings were observed by Gafurov *et al.* upon contacting $\gamma\text{-Al}_2\text{O}_3$ with anthraquinone, which were associated to a tetra-coordinated Al_{IV} pair.³⁹ This experiment with CO further supports the assignment of a unique reactive monomeric Cu(II) species (site I) for the selective conversion of CH_4 to CH_3OH . From the reactivity observed during the one-electron oxidation of carbon monoxide, one can probe the chemical surrounding of the active center. The formation of a bicarbonate radical along with the observed hyperfine coupling constant is consistent with the presence of a hydroxyl group and two equivalent Al_{IV} in the coordination sphere of the reactive Cu(II) center.

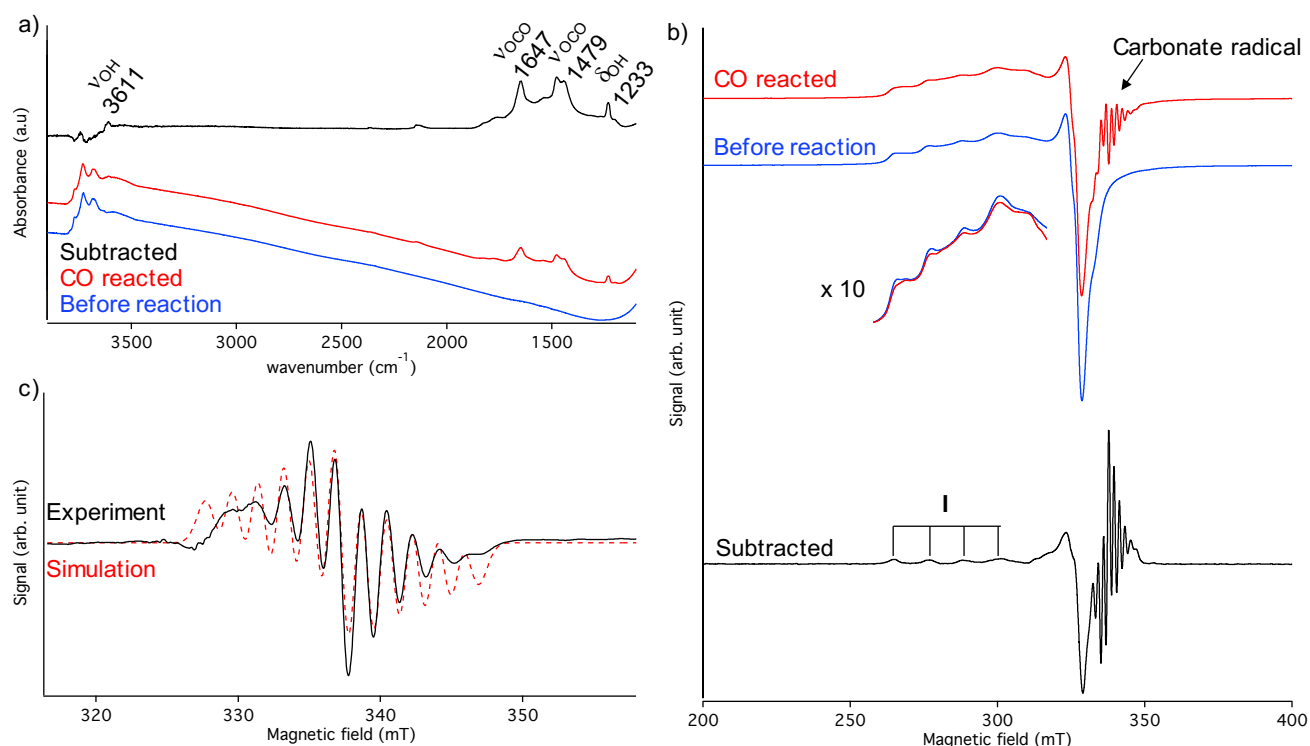


Figure 5. a) FTIR and b) X-band EPR spectra (298 K) of $\mathbf{1}_{500}\text{-}\eta\text{-a}_{500}$ before (blue) and after (red) reaction with 110 mbar of CO at room temperature and the corresponding difference spectrum (black). c) Extracted EPR signal of the carbonate radical formed upon reaction with CO (black) and simulation (dashed red) [$g_{\text{eff}} = 2.0026$ and $A_{\text{eff}} = 50 \text{ MHz}$].

We further investigated the reactive species (site I) in $\mathbf{1}_{500}\text{-}\eta\text{-a}_{500}$, which contains the highest amount of reactive Cu(II), with hyperfine sublevel correlation spectroscopy (HYSCORE)⁴⁰. Note that the inactive species (site II) are in fact silent in X-band HYSCORE spectra (see Fig. S36) such that this method allows for selective observation of the ^1H and ^{27}Al couplings of the reactive species. The HYSCORE spectrum of the reactive species, measured at the magnetic field position corresponding to the maximum intensity of the echo-detected EPR spectrum (Fig. 6a), reveals the presence of coupled ^1H nuclei in close proximity to the Cu(II) center, together with a distribution of ^{27}Al couplings (Fig. 6b). The HYSCORE spectrum of the reactive species was simulated (Fig. 6b & Fig. S35), assuming

the presence of two equivalent ^{27}Al nuclei, with the related hyperfine and quadrupole couplings of $a_{\text{iso}} = 3.39$ MHz, $a_{\text{dip}} = [-0.88 \ 0.03 \ 0.86]$ MHz, $P = -10.03$ MHz ($\eta = 0.185$). These parameters are quite close to both ^{27}Al hyperfine and quadrupole tensors, estimated for the molecular precursor **1** (see ESI Section 3). This indicates that the Al atoms of the reactive species possess similar symmetry and coordinative surrounding as in **1**. The ^1H hyperfine coupling in **1**₅₀₀- η -a₅₀₀ was simulated to be $a_{\text{iso}} = -0.5 \pm 0.5$ MHz, $a_{\text{dip}} = [-4.75 \pm 0.25; -4.75 \pm 0.25; 9.5 \pm 0.5]$ MHz, which corresponds to a Cu—H distance of 2.57 ± 0.05 Å within the point-dipole approximation. Such proton distance is attributed to the presence of hydroxyl group bound to the Cu(II) active sites.

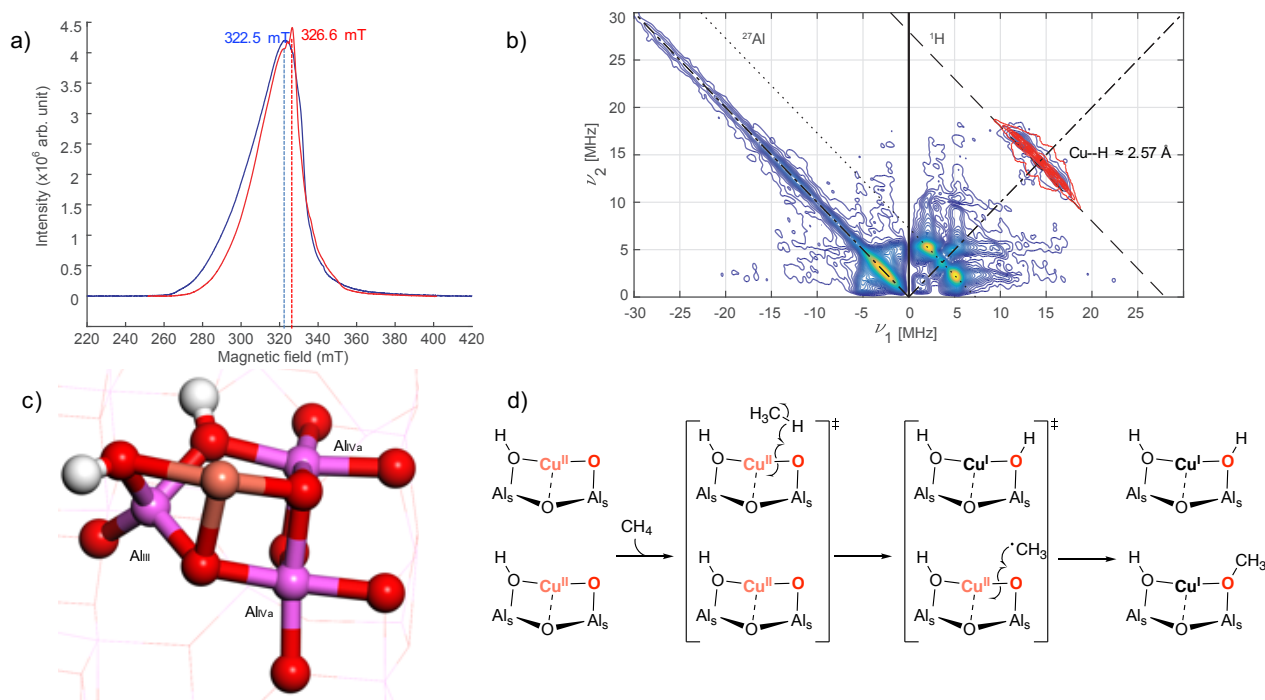


Figure 6. **a)** X-band echo detected spectra recorded at 10 K for supported catalysts before (**1**₅₀₀- η -a₅₀₀, red) and after reaction with CH₄ (**1**₅₀₀- η -a₅₀₀ reacted, blue). The dashed lines indicate the field position used to record the HYSCORE spectra. **b)** X-band HYSCORE spectrum of **1**₅₀₀- γ -Al₂O₃₋₅₀₀ at 10 K recorded at the field of 326.6 mT, sum of three spectra with $\tau = [280 \ 312 \ 400]$ ns. Spectral intensity along the antidiagonal of (→) quadrants is caused by phase cycling imperfection. Antidiagonal lines in the HYSCORE spectra indicate nuclear frequencies of ^1H (dashed) and ^{27}Al (dotted). The experimental spectrum is displayed in blue to yellow and the simulated ^1H ridge in red. **c)** DFT calculated structure of the reactive tricoordinated $[(\text{Al}_2\text{O})\text{CuO}(\text{OH})]^-$ site present on the (110) facet of $\gamma\text{-Al}_2\text{O}_3$. **d)** A possible 2 electron mechanism for CH₄ activation with 2 $[(\text{Al}_2\text{O})\text{CuO}(\text{OH})]^-$ through hydrogen abstraction followed reaction of the methyl radical.

The presence of a single, unique EPR signature for all reactive Cu(II) centers (site I) formed on different transition aluminas allows us to refine the geometrical configuration and surrounding environment of this center through combining the experimental evidences derived for the **1**₅₀₀- γ -Al₂O₃₋₅₀₀ and **1**₅₀₀- η -Al₂O₃₋₅₀₀ materials. The Cu(II) active sites have the following characteristics: i) they possess a coordinated hydroxyl group, ii) they are in close proximity to 2 equivalent Al_{IV} sites, as shown for γ - and η -Al₂O₃ and iii) their formation is correlated to the presence of highly Lewis acidic Al_{III} sites. Such features are strongly reminiscent of the structural characteristics of the (110) facet of $\gamma\text{-Al}_2\text{O}_3$,⁴¹ or the related structures formed at the edge between the (110) and (100) facets.⁴² We therefore

explored possible structures for the active sites that would feature a characteristic, nearly-axial EPR signature, as well as reasonable formation energies. These Cu(II) species were modelled by adsorbing a CuO fragment onto various partially hydroxylated configurations of the (110) facet of γ -Al₂O₃ (1 H₂O per unit cell or 3 OH.nm⁻² similar to the experimental OH density for γ -Al₂O₃₋₅₀₀ – 2.5 OH.nm⁻² – see ESI section 8, Figs. S37-39). Among these, one model meets all aforementioned experimentally determined requirements (see also Fig. S38, model s1a_1). This model corresponds to a tri-coordinated Cu(II)-oxo site coordinated to two equivalent Al_{IV} and an –OH bound to the so-called Al_{III} with a Cu---H distance of 2.76 Å (Fig. 6c). The Cu---H distance is slightly longer than the experimental value (2.76 Å compared to 2.57 Å), likely a result of the shallow potential energy surface. In particular, the T-shape geometry at Cu (Fig. 6c) is consistent with the EPR signature of the reactive species featuring a nearly axial *g* tensor.

Because the partial oxidation of CH₄ to CH₃OH is a two-electron process, two Cu(II) monomers must be involved since the Cu(II) sites are reduced to Cu(I) according to XANES and EPR spectroscopy. This process is feasible via an H-atom abstraction process on the hydroxyl or the oxo bound to Cu(II), generating an OH and a methyl radical that will generate a Cu(I) surface methoxy or CH₃OH species via reaction with a second Cu(II) site (Fig. 6d).

Conclusion

Overall, this study shows that alumina is able to stabilize highly reactive isolated Cu(II) sites. EPR spectroscopy is shown here to be a particularly powerful characterization method, allowing the exclusive detection of the reactive monomeric sites involved in the partial oxidation of CH₄. The detection of a specific EPR signature for such active sites, [(Al₂O)CuO(OH)]⁻, which adopt a T-shape structure, is particularly noteworthy as it opens ways to tailor materials that can stabilize such type of structures. We are currently investigating alternative supports that could stabilize such species with the aim to increase the density of reactive sites.

Acknowledgements

J.M. and M.A.N. thank Shell Global Solutions International B.V. for financial support. We acknowledge Elettra Sincrotrone Trieste for providing access to its synchrotron radiation facilities and we thank Giuliana Aquilanti, Luca Olivi and Danilo Oliveira de Souza for assistance in using XAFS beamline. J.M. acknowledges Dr. Z. Berkson and Dr. D. Mance for their help conducting and analyzing the NMR experiments.

References

1. Lange, J. P., De Jong, K. P., Ansorge, J. & Tijm, P. J. A. Keys to methane conversion technologies. *Stud. Surf. Sci. Catal.* **107**, 81–86 (1997).
2. Ahlquist, M., Nielsen, R. J., Periana, R. A. & Goddard, W. A. Product protection, the key to developing high performance methane selective oxidation catalysts. *J. Am. Chem. Soc.* **131**, 17110–17115 (2009).
3. Ravi, M., Ranocchiari, M. & van Bokhoven, J. A. The Direct Catalytic Oxidation of Methane to Methanol—A Critical Assessment. *Angew. Chemie - Int. Ed.* **56**, 16464–16483 (2017).
4. Latimer, A. A., Kakekhani, A., Kulkarni, A. R. & Nørskov, J. K. Direct Methane to Methanol: The Selectivity-Conversion Limit and Design Strategies. *ACS Catal.* **8**, 6894–6907 (2018).

- 291 5. Lawton, T. J. & Rosenzweig, A. C. Methane-Oxidizing Enzymes: An Upstream Problem in Biological Gas-to-
292 Liquids Conversion. *J. Am. Chem. Soc.* **138**, 9327–9340 (2016).
- 293 6. Chan, S. I. *et al.* Redox potentiometry studies of particulate methane monooxygenase: Support for a trinuclear
294 copper cluster active site. *Angew. Chemie - Int. Ed.* **46**, 1992–1994 (2007).
- 295 7. Balasubramanian, R. *et al.* Oxidation of methane by a biological dicopper centre. *Nature* **465**, 115–119 (2010).
- 296 8. Ross, M. O. *et al.* Particulate methane monooxygenase contains only mononuclear copper centers. *Science (80-
297).* **364**, 566–570 (2019).
- 298 9. Lieberman, R. L. & Rosenzweig, A. C. Crystal structure of a membrane-bound metalloenzyme that catalyses the
299 biological oxidation of methane. *Nature* **434**, 177–182 (2005).
- 300 10. Starokon, E. V., Parfenov, M. V., Pirutko, L. V., Abornev, S. I. & Panov, G. I. Room-temperature oxidation of
301 methane by α -oxygen and extraction of products from the FeZSM-5 surface. *J. Phys. Chem. C* **115**, 2155–2161
302 (2011).
- 303 11. Groothaert, M. H., Smeets, P. J., Sels, B. F., Jacobs, P. A. & Schoonheydt, R. A. Selective oxidation of methane by the
304 bis(μ -oxo)dicopper core stabilized on ZSM-5 and mordenite zeolites. *J. Am. Chem. Soc.* **127**, 1394–1395 (2005).
- 305 12. Newton, M. A., Knorpp, A. J., Sushkevich, V. L., Palagin, D. & Van Bokhoven, J. A. Active sites and mechanisms in
306 the direct conversion of methane to methanol using Cu in zeolitic hosts: A critical examination. *Chem. Soc. Rev.*
307 **49**, 1449–1486 (2020).
- 308 13. Woertink, J. S. *et al.* A [Cu₂O]₂²⁺ core in Cu-ZSM-5, the active site in the oxidation of methane to methanol. *Proc.
309 Natl. Acad. Sci. U. S. A.* **106**, 18908–18913 (2009).
- 310 14. Grundner, S. *et al.* Single-site trinuclear copper oxygen clusters in mordenite for selective conversion of methane
311 to methanol. *Nat. Commun.* **6**, 7546 (2015).
- 312 15. Kulkarni, A. R., Zhao, Z. J., Siahrostami, S., Nørskov, J. K. & Studt, F. Monocopper Active Site for Partial Methane
313 Oxidation in Cu-Exchanged 8MR Zeolites. *ACS Catal.* **6**, 6531–6536 (2016).
- 314 16. Sushkevich, V. L., Palagin, D. & van Bokhoven, J. A. The Effect of the Active-Site Structure on the Activity of Copper
315 Mordenite in the Aerobic and Anaerobic Conversion of Methane into Methanol. *Angew. Chemie - Int. Ed.* **57**,
316 8906–8910 (2018).
- 317 17. Knorpp, A. *et al.* Paired copper monomers in zeolite omega: the active site for methane-to-methanol conversion.
318 *Angew. Chemie Int. Ed.* anie.202014030 (2020). doi:10.1002/anie.202014030
- 319 18. Pappas, D. K. *et al.* The Nuclearity of the Active Site for Methane to Methanol Conversion in Cu-Mordenite: A
320 Quantitative Assessment. *J. Am. Chem. Soc.* **140**, 15270–15278 (2018).
- 321 19. Lange, J. P., Sushkevich, V. L., Knorpp, A. J. & Van Bokhoven, J. A. Methane-to-Methanol via Chemical Looping:
322 Economic Potential and Guidance for Future Research. *Ind. Eng. Chem. Res.* acs.iecr.9b01407 (2019).
323 doi:10.1021/acs.iecr.9b01407
- 324 20. Jovanovic, Z. R. *et al.* Oxidation of methane to methanol over Cu-exchanged zeolites: Scientia gratia scientiae or
325 paradigm shift in natural gas valorization? *J. Catal.* **385**, 238–245 (2020).
- 326 21. Le, H. V. *et al.* Stepwise Methane-to-Methanol Conversion on CuO/SBA-15. *Chem. - A Eur. J.* **24**, 12592–12599
327 (2018).

- 328 22. Bozbag, S. E. *et al.* Direct Stepwise Oxidation of Methane to Methanol over Cu-SiO₂. *ACS Catal.* **8**, 5721–5731
329 (2018).
- 330 23. Wang, X. *et al.* Copper-modified zeolites and silica for conversion of methane to methanol. *Catalysts* **8**, 545
331 (2018).
- 332 24. Meyet, J. *et al.* Monomeric Copper(II) Sites Supported on Alumina Selectively Convert Methane to Methanol.
333 *Angew. Chemie - Int. Ed.* **58**, 9841–9845 (2019).
- 334 25. Copéret, C. Fuels and energy carriers from single-site catalysts prepared via surface organometallic chemistry.
335 *Nature Energy* **4**, 1018–1024 (2019).
- 336 26. Veith, M., Valtchev, K. & Huch, V. Tetraalkoxyaluminates of nickel(II), copper(II), and copper(I). *Inorg. Chem.* **47**,
337 1204–1217 (2008).
- 338 27. Jang, H. J., Keith Hall, W. & D'Itri, J. L. Redox behavior of CuZSM-5 Catalysts: FTIR investigations of reactions of
339 adsorbed NO and CO. *J. Phys. Chem.* **100**, 9416–9420 (1996).
- 340 28. Sushkevich, V. L. & Van Bokhoven, J. A. Revisiting copper reduction in zeolites: The impact of autoreduction and
341 sample synthesis procedure. *Chem. Commun.* **54**, 7447–7450 (2018).
- 342 29. Beebe, T. P., Crowell, J. E. & Yates, J. T. Infrared spectroscopic study of the rotation of chemisorbed methoxy
343 species on an alumina surface. *J. Chem. Phys.* **92**, 5119–5126 (1990).
- 344 30. Comas Vives, A., Schwarzwälder, M., Copéret, C. & Sautet, P. Carbon carbon bond formation by activation of CH₃F
345 on alumina. *J. Phys. Chem. C* **119**, 7156–7163 (2015).
- 346 31. Newton, M. A. *et al.* On the Mechanism Underlying the Direct Conversion of Methane to Methanol by Copper
347 Hosted in Zeolites; Braiding Cu K-Edge XANES and Reactivity Studies. *J. Am. Chem. Soc.* **140**, 10090–10093
348 (2018).
- 349 32. Godiksen, A. *et al.* Coordination environment of copper sites in Cu-CHA zeolite investigated by electron
350 paramagnetic resonance. *J. Phys. Chem. C* **118**, 23126–23138 (2014).
- 351 33. Busca, G. Structural, Surface, and Catalytic Properties of Aluminas. *Adv. Catal.* **57**, 319–404 (2014).
- 352 34. Maciver, D. S., Tobin, H. H. & Barth, R. T. Catalytic aluminas I. Surface chemistry of eta and gamma alumina. *J.*
353 *Catal.* **2**, 485–497 (1963).
- 354 35. Zubkov, S. A., Borovkov, V. Y., Gagarin, S. G. & Kazansky, V. B. Infrared study of nitrogen adsorption on alumina.
355 *Chem. Phys. Lett.* **107**, 337–340 (1984).
- 356 36. Wischert, R., Copéret, C., Delbecq, F. & Sautet, P. Dinitrogen: A selective probe for tri-coordinate Al “defect” sites
357 on alumina. *Chem. Commun.* **47**, 4890–4892 (2011).
- 358 37. Wischert, R., Laurent, P., Copéret, C., Delbecq, F. & Sautet, P. γ -Alumina: The Essential and Unexpected Role of
359 Water for the Structure, Stability, and Reactivity of “Defect” Sites. *J. Am. Chem. Soc.* **134**, 14430–14449 (2012).
- 360 38. Szanyi, J. & Kwak, J. H. Dissecting the steps of CO₂ reduction: 1. The interaction of CO and CO₂ with γ -Al₂O₃: An
361 in situ FTIR study. *Phys. Chem. Chem. Phys.* **16**, 15117–15125 (2014).
- 362 39. Gafurov, M. R. *et al.* Quantitative Analysis of Lewis Acid Centers of γ -Alumina by Using EPR of the Adsorbed
363 Anthraquinone as a Probe Molecule: Comparison with the Pyridine, Carbon Monoxide IR, and TPD of Ammonia.
364 *J. Phys. Chem. C* **119**, 27410–27415 (2015).

- 365 40. Höfer, P., Grupp, A., Nebenführ, H. & Mehring, M. Hyperfine sublevel correlation (hyscore) spectroscopy: a 2D
366 ESR investigation of the squaric acid radical. *Chem. Phys. Lett.* **132**, 279–282 (1986).
- 367 41. Digne, M., Sautet, P., Raybaud, P., Euzen, P. & Toulhoat, H. Hydroxyl Groups on γ -Alumina Surfaces: A DFT Study.
368 *J. Catal.* **211**, 1–5 (2002).
- 369 42. Batista, A. T. F. *et al.* Beyond γ -Al₂O₃ crystallite surfaces: The hidden features of edges revealed by solid-state
370 ¹H NMR and DFT calculations. *J. Catal.* **378**, 140–143 (2019).
- 371